Neural integration underlying a time-compensated sun compass in the migratory monarch butterfly

Eli Shlizerman[1], James Phillips-Portillo[2], Daniel B. Forger[3*], Steven M. Reppert[2]

1 Department of Applied Mathematics, Department of Electrical Engineering, University of Washington, Seattle, WA, 98195, USA
2 Department of Neurobiology, University of Massachusetts Medical School, Worcester, MA, 01605, USA
3 Department of Mathematics, Department of Computational Medicine and Bioinformatics, University of Michigan, Ann Arbor, MI, 48104, USA
* Corresponding Author

Abstract

Migrating Eastern North American monarch butterflies use a time-compensated sun compass to adjust their flight to the southwest direction. While the antennal genetic circadian clock and the azimuth of the sun are instrumental for proper function of the compass, it is unclear how these signals are represented on a neuronal level and how they are integrated to produce flight control. To address these questions, we constructed a receptive field model of the compound eye that encodes the solar azimuth. We then derived a neural circuit model, which integrates azimuthal and circadian signals to correct flight direction. The model demonstrates an integration mechanism, which produces robust trajectories reaching the southwest regardless of the time of day and includes a configuration for remigration. Comparison of model simulations with flight trajectories of butterflies in a flight simulator shows analogous behaviors and affirms the prediction that midday is the optimal time for migratory flight.

1 Introduction

Each fall, eastern North American monarch butterflies (*Danaus plexippus*) fly up to 4000 km to specific overwintering sites in Central Mexico. Throughout this journey monarchs constantly correct their flight direction to maintain a southerly orientation. Laboratory observations from a flight simulator, capable of tracking flight direction, show that migrant monarchs orient towards the southwest (SW) direction by visual cues, relying primarily on the horizontal (azimuthal) position of the sun (Mouritsen & Frost 2002; Froy et al. 2003; Zhu et al. 2009; Merlin et al. 2009; Guerra et al. 2012). Migrants use their circadian clocks to compensate for the changing sun position and thereby maintain a fixed flight bearing.

1

Monarch antennae contain an intracellular, light-sensitive clock mechanism which has been shown to be responsible for calibrating the sun compass (Merlin et al. 2009). As in *Drosophila* and mice, the primary molecular mechanism of the monarch clock is an autoregulatory transcriptional feedback loop. In the monarch, the feedback loop utilizes two distinct cryptochromes (CRYs), a blue light circadian photoreceptor (CRY1) and a transcriptional repressor (CRY2), transcription factors CLOCK (CLK) and CYCLE (CYC) that drive the transcription of the *period (per)*, *timeless (tim)*, and *cry2* genes, which are translated into PER, TIM, and CRY2 proteins, respectively (Zhu et al. 2008).

While the monarch time-compensation clocks are housed in the antennae, the sun's azimuthal position is detected by the eyes. Neuronal signals originating from photoreceptors in each ommatidial unit of the compound eye are processed by several optic neuropils before they are relayed to the central brain. A main target for visual neurons in the central brain is the anterior optic tubercle (AoTU), a structure that is connected to the Central Complex (CX), the presumed site of the sun compass (Heinze et al. 2013; Heinze & Reppert 2012). Within the CX, the lateral accessory lobes (LALs) are of particular relevance because neurons within them connect to descending motor pathways that ultimately control behavior. A long-standing, fundamental question about monarch migration has been how the circadian clock interacts with the changing position of the sun to form a time-compensated sun compass that directs flight? Here we propose a neuronal model for both encoding of the sun's azimuthal position, and molecular timekeeping signals and how they can be compared to form a time-compensated sun compass. Our results propose a simple neural mechanism capable of producing a robust time-compensated sun compass navigation system through which monarch butterflies could maintain a constant heading during their migratory flight.

Results

A basic assumption of our model is that time and solar signals are encoded by neuronal firing rate. This allows us to propose a mechanism, which uses a small number of neurons, to compare the firing rate of azimuthal neurons, responding to the luminance detected by the eyes, with neurons whose firing rate shows a circadian rhythm, as seen in "clock" neurons in other

species, (e.g., Colwell 2011; Belle et al. 2009) and as an outcome directs flight. We first define the neural input signals into such a mechanism.

For neural representation of the clock, we postulate two neurons, NCLK1 and NCLK2, whose firing-rates oscillate in accordance with two primary molecular oscillations generated by the monarch circadian clock (**Fig. 1**A_1) (Merlin et al. 2009). NCLK1 is linked to the oscillations of *cry2* transcription factor through a neuron called NCLK1_C. In the absence of input, NCLK1 fires with constant background firing rate (BG) and receives inhibitory input from NCLK1_C that follows oscillations of *cry2* ($NCLK1 = BG - NCLK1\_C$). As a result, the NCLK1 firing-rate is anti-phase to the oscillation pattern of *cry2*. NCLK2 follows the oscillation pattern of *per/tim* transcription factors directly (**Fig. 1**A_3). Analogously we introduce a neuron labeled NCLK2_C with a firing rate that is anti-phase to the oscillation patterns found in NCLK2 and *per/tim.*. These links between neural and molecular representations of the circadian rhythm are motivated by recent work describing the neuronal activity of clock neurons in various species (DeWoskin et al. 2015; Myung et al. 2015; Ukai-Tadenuma et al. 2008). The particular configuration of these links is phenomenological and aimed to show that a neural mechanism from molecular rhythms to firing rate with these phase relationships could exist.

Each of the firing-rate curves is non-monotonic, that is, they do not produce a unique firing rate during the daylight hours. This property precludes a single curve from being used to identify the time of day. However, we note that due to the 6-hour phase shift between the curves, a simple correction for this ambiguity could be to consider a sum of the NCLK1 and NCLK2 curves, which produces a monotonic curve. To gain further information on electrical signals possibly related to the circadian clock we performed electro-antennogram (EAG) recordings over the course of several days under normal light/dark (L:D) conditions (see *SMM*). Frequency analysis of the electrical activity suggests that intrinsic antennal electrical activity increases during the day and decreases during the night, illustrated in **Fig. 1**A_2. During the day, when the sun compass is active, the signal power curve appears to be non-monotonic with lowest activity at $T = 0$ and a peak near mid afternoon $at\ T = 8$. This is surprisingly similar to the predicted activity of NCLK1. Non-monotonicity of the electric antennal signal has been also detected in *Drosophila* (Tanoue et al. 2004).

For neural encoding of the solar azimuth we consider neurons with visual receptive fields carrying information from the compound eye. A simple and robust way for detecting the solar azimuth is integration of luminance captured by all ommatidia in a wide receptive field that a neuron subtends (see **Fig. 1**B and *SMM*). We note that when the eyes are modeled as two hemispheres separated by 180°, as approximately appears in the monarch, integration of the luminance from a single eye indeed provides azimuthal information, however, in just one Cartesian direction. This implies that azimuth detection is ambiguous. For example, azimuthal sun positions in front and behind the animal would yield the same integrated luminance in both left and right eye (**Fig. 1**B$_1$). A simple and sufficient way to measure the solar position in two Cartesian dimensions would be to consider receptive fields arranged 90° apart instead of 180°, implying that the solar azimuth is minimally encoded with two rhythms. We follow this reasoning and introduce two types of neurons, NS1 and NS2, with the simplest anatomical arrangement of receptive fields that allow unambiguous encoding of solar azimuth. The receptive field of NS1 comprises all ommatidia in a single eye (e.g. right eye) and its firing-rate is proportional to the integrated luminance signal of the eye it subtends. NS2 neuron has a receptive field composed of two quadrants of the two eyes (e.g. frontal hemisphere) and will produce a luminance signal and firing rate curve shifted by 90° relative to the NS1 response, see **Fig. 1**B$_2$. The curves that we propose have been described in the insect visual system. Similar curves were obtained from recordings from *Drosophila* lobular plate tangential neurons (H and V neurons) (Neri 2006). Further, recent studies in monarchs and other insects have documented single, wide receptive field tangential neurons with dendrites that cover the whole lobula plate (Heinze et al. 2013). We expect NS1 and NS2 neurons to be of a similar type.

To propose a mechanism for integration of clock and azimuth neural signals into a time-compensated sun compass, we introduce two control neurons, whose firing rate is denoted by f_l and f_r. These neurons receive clock and azimuth signals and match them according to a particular wiring, denoted as I_l and I_r, to indicate whether a current flight angle is correct, or whether to steer toward left (f_l) or right (f_r) directions. We then propose the following equations for modeling the firing rates of left and right control neurons

$$\frac{df_l}{dt} = -\alpha f_l + \beta \varphi(I_l), \qquad \varphi(x) = \begin{cases} 0 & x < 0, \\ x & x \geq 0. \end{cases} \qquad (1)$$
$$\frac{df_r}{dt} = -\alpha f_r + \beta \varphi(I_r),$$

The parameter α denotes the decay rate of the firing-rate in the absence of input and $\beta\varphi(x)$ denotes that only positive inputs elicit response. Since neurons can encode motion, we assume that input wirings I_l and I_r correspond to the force used for steering and the firing rates will indicate the angular velocity used by the monarch for correction in each direction. Given the axisymmetric anatomy of the monarch, it is reasonable to assume that there are two parallel pathways, controlling leftward and rightward turns. Generally, in insect flight, turns come from opposite forces being applied to the left and right wings. Similarly, in our model the total angular velocity is represented by the difference between left and right firing-rate units

$$F = f_l - f_r = \frac{dA}{dt},$$ (2)

with A representing the azimuthal angle between the sun's position and the SW. We note that although the system in (1) was derived based on neural firing rate principles, it is directly related to flight commands, as it is analogous to a formalism based on Newton's first law (Bergou et al. 2010)

$$m\frac{d^2A}{dt^2} + v\frac{dA}{dt} = I.$$ (3)

in which the force (I) equals the mass times the acceleration and a damping coefficient (v) times the angular velocity. In our model, F represents dA/dt such that the system in (1) is equivalent to the system in (3). F positive designates correction to the left and F negative designates correction to the right. When the flight angle relative to the sun is correct, the firing rates of the two units will be equal and $F = 0$. We define this state as the *balanced state* (fixed point).

For the integration mechanism to be viable it has to maintain the balanced state once achieved. Because the solar azimuth increases approximately linearly over the day (**Fig. 2**A$_1$) the balanced state is represented as a line (A_{fp}) in a plane consisting of the time of day (T) and the azimuthal angle (A). We require that the integration mechanism will return to the balanced state at any time (T), i.e., requiring the system in (1) to implement A_{fp} as a line attractor (**Fig. 2**A$_2$)(Amit 1992). We then ask, for the given firing rate curves of clock neurons NCLK1, NCLK2 and azimuth neurons NS1, NS2, what are the input wirings I_l and I_r that implement such a mechanism? We address this question by deriving a potential function $V(A, T)$ (see *SMM* for the derivation) which specifies the conditions for testing given clock and azimuth wirings, as to whether the line A_{fp} is a line attractor, and we use it to detect candidate integration mechanisms. From this formalism we first note that straightforward matching of single clock and

sun signals (e.g., NCLK1 and NS1), the simplest candidate mechanism, will not satisfy the required conditions, as this results in multiple balanced states. Alternatively, we find that matching all four signals, in a particular way, such that the left unit subtracts the sun azimuth inputs from the clock inputs, and the right unit implements the opposite

$$I_l = D_1 + D_2, \qquad\qquad D_1 = NCLK1 - NS1, \qquad D_2 = NCLK2 - NS2,$$
$$I_r = -D_1 - D_2 = -I_l,$$
(4)

will satisfy the derived conditions. We illustrate this input wiring and the associated potential function $V(A, T)$ in **Fig. 2**A$_{3,4}$. We also show that for the specified input signals and their addition or subtraction (256 variations), this is the *only wiring* possibility that produces a robust flight direction for the duration of the day (see *SMM*).

In addition to the line attractor, there is another solution (fixed flight angle) that satisfies the equation $F = 0$. Stability analysis of this fixed point shows that it is unstable, and as such serves as a separatrix; trajectories initiated near it are being repelled from it. The balanced state and the separatrix merge at the SW direction, at $T = 0$ and $T = 12$, and become apart with maximal separation at $T = 6$ (**Fig. 2**A$_5$). For further insight, we performed inceptive intracellular recordings from interneurons within the LALs responding to rotating light stimuli at different times of day. We find the recorded firing rates sensitive to time (firing rate increases with time), azimuthal position of the light, and rotation direction. By taking the difference between clockwise (left) and counter-clockwise (right) rotation responses, as in (Tammero et al. 2004), and comparing the outcome with F, we observe some qualitative features that our model indicates, in particular, presence of fixed points, and opposite signals in between the fixed points (see Fig. S1).

Our formalism allows us to examine rewiring of input signals (e.g. inclusion of NCLK1_C and NCLK2_C) to test whether the modified circuit could support other stable directions. We find that such a configuration exists; when clock input signals NCLK1, NCLK2 are replaced by NCLK1_C and NCLK2_C and the connections are flipped (excitatory connections become inhibitory and vice versa), the circuit will implement a stable northeast (NE) flight for the whole light phase of the day (**Fig. 2**B$_1$). This mechanism is also unique as the mechanism for SW flight. We thus conclude that for all neural input signals that we defined in **Fig. 1**, the wirings, depicted in **Fig. 2**, are the only two stable plausible mechanisms. As such the integration supports only two flight

directions: SW or NE. Remarkably, the NE flight direction is actually used by remigrant monarchs in the spring (Guerra & Reppert 2013).

To simulate the time-compensated sun compass we use the control units model (1), which produces the signal F (angular velocity) and compute the angular position A from it (2). The outcome is a `self-correcting' model in which the simulated dynamics (flight tracks) converge to the balanced state from any initial angular position (except the degenerate case of zero velocity exactly at the separatrix). The transient dynamics, however, will depend on the choice of the parameter α, initial angular position A, and initial velocities f_l and f_r. We explore these dynamics by computational simulations and compare them with experimental flight paths recorded during tethered flight (Guerra et al. 2012; Merlin et al. 2009) in which dynamical features have not been analyzed before. As a particular example, we illustrate the convergence to the balanced state for two scenarios, morning and afternoon (**Fig. 3 and SV**). When the simulations are initiated with zero angular velocity, the dynamics follow the direction that does not require separatrix crossing. These trajectories may reach the balanced state at different times and with nonzero velocity, continue beyond it, change their direction and return back to the fixed point with slower velocity in opposite direction exhibiting "ease-in" dynamics to the balanced state. Indeed such dynamics are characteristic to butterflies in a flight simulator (as we show in **Fig. 4**C and observed in (Merlin et al. 2009; Mouritsen & Frost 2002)).

To determine the time it takes for the angular position to settle to the SW, we set the angular velocity to zero, and initialize simulations from various angular positions (**Fig. 4**A). During afternoon (ZT=4:8) average convergence time is on the order of $10\ sec$ ($\pm 8\ sec$). However, for morning and evening times, we observe much slower convergence, with average times of about $30\ \sec$ ($\pm 25\ sec$). To further explore this variance we depict the spatial distribution of convergence times. In the afternoon, most trajectories (except near the separatrix) quickly converge to the SW. However, in the morning and in the evening, slow convergence is extended up to a semi-circle, which includes the separatrix. Slow convergence in this region stems from angular acceleration being small, hindering the trajectory to gain velocity. Our model, therefore, predicts that there is a difference in convergence timescales between control and clock-shifted tracks recorded in the afternoon. In particular, we expect clock-shifted tracks to be scattered in the slow convergence region. Such behaviors are typical for clock-shifted tracks recordings as reported in (Guerra et al. 2012; Merlin et al. 2009) and depicted in **Fig. 4**D, **Fig. S 4.**

7

A central feature in our model is the separatrix, which determines the time and the directionality of the flight correction to the SW. We therefore validate its existence by analyzing the changes in directions (turns and rotations) in experimental flight track data (4 tracks spanning 32 minutes of flight), see **Fig. 4**B, **Fig. S 4.** We find that turns (extreme points of slope > 0.01, farther than $20°$ from the SW) are frequent and appear more regularly than rotations. Their distribution is dense near the SW and becomes sparse as distance from the SW increases. Particularly, we do not identify any turns in the interval $80 - 110°$, the predicted location of the separatrix (positioned at $105°$ at $ZT = 8$), and the density in the right correction interval is higher than in the left interval, another feature of the asymmetric position of the separatrix. The directionality of turns is consistent with the predicted left and right correction regions in our model, indicating that turns in flight tracks are in accord with the correction response of the model. From analysis of rotations, defined as trajectories that cross the separatrix region, we observe that they typically occur in clusters (with average of 3 rotations per cluster), and occurrence of turns during rotations significantly decreases. Indeed, our model indicates that once the trajectory crosses the separatrix, the correction direction is alternated, making a full rotation to be favorable than a turn against the correction direction. To infer the location of the separatrix, we compute the positions from which full rotations are more probable. We find that positions in the region of $80 - 140°$ have the highest probability to perform a rotation, with a peak of $P = 0.7$ at $110 - 115°$ bin. Remarkably, this position is in close agreement with the model prediction.

Since the compass is being activated by changes in the course of flight, we examine the model's behavior in the presence of input noise. When perturbations originate from white noise (e.g. due to cloudiness), the trajectory once converged will hover around the SW a radius proportional to the magnitude of the perturbations. Incorporating occasional kicks in the model, that simulate strong perturbations, for example caused by wind bursts, occlusions or effects of tethering, the angular position may rapidly diverge from the fixed point, as we indeed observe in recordings (**Fig. 4**D). In such a case, the trajectory could cross the separatrix and exhibit a full rotation or several rotations before settling to the fixed point. Our model indicates that compass sensitivity to such behaviors depends on the distance between the SW and the separatrix, which is minimal in the morning and evening and maximal in the middle of the day. Therefore,

we expect that monarchs are more prone to frequent rotations due to strong perturbations in the morning and evening than in the middle of the day (see **SV**).

When we compare traces produced by model simulations that included noise and flight tracks of tethered migrants we find similar behaviors (**Fig. 4**C,D purple vs. orange). By examining short time navigation (on the order of seconds) we observe common small displacements from the SW angle, large displacements that cause full rotation and ease-in convergence to the SW angle in both the model and the experiment (**Fig. 4**C). For long periods of flight (order of minutes), we have also compared the distributions of angular position and velocity. The comparison is done for flight data (recorded during noon-2pm time window, i.e. $ZT = 6 - 8$) with normal L:D cycle and with 6h delayed L:D cycle (**Fig. 4**D). For normal L:D cycle the distribution of the angular velocity in the model and experiments shows that the velocities are small near the stable fixed point and large at half circle distance from it. For the shifted L:D cycle we expect the trajectory to converge to the NW direction (SW direction rotated by 90°). Tethered simulator tracks indeed show that the trajectory is rotated, and in addition to rotation, the trajectory is noisier and slowly drifting toward the N and NE directions. In the model, we adjust the clock input by shifting NCLK1 and NCLK2 backward, which sets the compass model to morning time ($ZT \approx 2$). The separatrix is then closer to the balanced state and the velocity of returning back to the balanced state is asymmetric, as shown in (**Fig. 4**A), and indicated in model and experiment angular velocity distributions. This produces a similar drift when we add noise to our model simulations (**Fig. 4**D bottom).

6 Discussion

The remarkable ability of monarch butterflies to migrate for thousands of miles while keeping the southerly direction suggests that they posses a neural circuit capable to integrate time of day and sun's position into a compass useful for navigation. Here we derived a model that matches the firing rate of clock and azimuth neural signals to provide angular position control. We show that there are two fixed points in the model, one is stable and corresponds to the SW direction and the other is unstable and divides the rotation direction. Simulating trajectories in the model

and comparing them with flight trajectories recorded from butterflies flying in a tethered simulator we find similar flight behaviors and distribution characteristics.

We propose two neural circuit components that allow us to construct the compass model. The first component is the azimuth encoding model implemented by receptive fields covering left/right and front/back hemispheres. Such receptive field arrangement shows that azimuth can be computed directly from sunlight intensity based on Lambert's law, does not require complex receptive fields or polarization patterns, and is robust to natural overcasts and shadows, as opposed to mechanisms based on small subsets of neurons (**Fig. S 3**). The second component that we introduce is the derivation of integration wiring for flight control. We discovered that straightforward matching integration (NCLK1 and NS1) is incompatible with the uniqueness condition of the balanced state. However, a single integration configuration based on phase shifted signals NCLK1, NS1 and NCLK2, NS2 will provide unique control. Simulations of the model confirm this analysis.

Comparison of flight tracks recorded in an outdoor flight simulator with tracks produced by our model confirms the existence of two correction regions separated by a separatrix, whose position is in close agreement with our model. Additionally, our model predicts extra sensitivity to perturbations in morning and evening times and those can cause a drift in a specific range of angles. We indeed observe sensitivity and drifts in flight trajectories of butterflies with shifted L:D cycles, in which flight was recorded in the afternoon but corresponds to morning time. Furthermore, by comparing short and long time segments of correction dynamics we find similarity in flight dynamics patterns, exhibited by ease-in, turns and full rotations and an accord between the distributions of angular velocities and position. These findings suggest that when the monarch loses its course it rotates back with velocity proportional to the curves of F described by our model.

In summary, our results indicate that both time-of-day and sun's azimuthal position can be encoded using firing-rate curves. These curves provide robust non-monotonic signals for integration of clock and visual cues into flight steering control. The neural circuit and conditions that we derive show that only a specific matching strategy will guarantee reaching the SW from almost any heading at any time of day. We also propose a rewiring that can support the NE bearing found in monarchs re-migrating out of Mexico in the spring (Guerra & Reppert 2013)

and show that these are the only two plausible strategies for fixed flight direction. The model that we have built closes the loop between the time and azimuth stimuli, and orientation control. As such, it provides an important framework for future studies of the monarch sun-compass. Our framework can be used to design electrophysiological and flight recordings experiments to compare responses in monarchs' neurons and model units and to determine the detailed architecture of neural circuits that implement the integration mechanism postulated by our model. It also provides a simple mechanism for navigation that can be used in devices that do not have the benefit of GPS.

Methods

Integration Model

Sensory azimuth and time encoding signals (expressed by computational neurons) are defined as the following functions $NS1(A) = \frac{I_b}{2}\left(1 - \sin\frac{A\pi}{180}\right), NS2(A) = \frac{I_b}{2}\left(1 + \cos\frac{A\pi}{180}\right), NCLK1(T) = \frac{I_b}{2}\left(1 - \cos\frac{\pi(T+3)}{12}\right), NCLK2(T) = \frac{I_b}{2}\left(1 - \sin\frac{\pi(T+3)}{12}\right),$ where I_b is set to 40Hz. The azimuth function is determined from half sphere model of the eyes while the clock function is determined according to recordings from antennae, molecular curves and requiring these signals to match in peak and trough amplitudes. Potential (Lyapunov) function used to determine the stability of the integration mechanism in Eq. (4) is defined as $V(A;T) = (\varphi(I_l) - \varphi(I_r))^2$. See further details in the SMM. Simulations of the model were performed using Mathworks MATLAB with our implementation of Euler-Muryama stochastic integrator.

Experimental Methods

Electroantennograms (EAGs) were recorded as the potential difference between the tip of the antenna and a specially designed head capsule, over the course of several (4-5) days under normal L:D conditions. To exclude olfactory and mechanosensory signals antennae were coated with transparent paint (Guerra et al., 2012; Merlin et al., 2009). EAG signals were sampled for 10 min every hour for the duration of the recording period and analyzed using fast Fourier transform to determine the relative power at all frequencies above 65 Hz.

Intracellular recordings from the CX were conducted during the light phase of each animals light dark cycle. For recordings, animals with a head capsule were mounted in the experimental

setup and aligned such that the LED stimulating apparatus was directly above the head and the recording electrode could access the brain frontally. The LALs were chosen as the target recording site because they receive both projections from the visual neuropils and from the central complex, the collection of midline neuropils thought to serve as the substrate for sun compass integration (Heinze & Reppert 2011). Intrinsic LAL-LAL neurons were found to be sensitive to the azimuthal position of the light source. They have been ordered by the Zeitgeber time at which the recording was performed. In analysis, background-firing rates were determined from intervals of no stimulus and difference between left and right rotation responses was computed for comparison with F, the output of the model. See further details in the SMM.

Acknowledgements

Authors Contributions

Conceptualization S.M.R., D.B.F and E.S.; Methodology E.S., D.B.F., J.P-P., and S.M.R.; Validation E.S. and J.P-P.; Formal Analysis E.S. and D.B.F.; Experiments J.P-P. and S.M.R; Writing – Original Draft E.S.; Writing – Review & Editing E.S., J.P-P., D.B.F., and S.M.R.; Funding Acquisition S.M.R., D.B.F. and E.S.

References

Amit, D.J., 1992. *Modeling brain function: The world of attractor neural networks*, Cambridge University Press.

Bahl, A. et al., 2013. Object tracking in motion-blind flies. *Nature neuroscience*, 16(6), pp.730–738.

Belle, M.D.C. et al., 2009. Daily electrical silencing in the mammalian circadian clock. *Science*, 326(5950), pp.281–284.

Bergou, A.J. et al., 2010. Fruit flies modulate passive wing pitching to generate in-flight turns. *Physical review letters*, 104(14), p.148101.

Colwell, C.S., 2011. Linking neural activity and molecular oscillations in the SCN. *Nature Reviews Neuroscience*, 12(10), pp.553–569.

DeWoskin, D. et al., 2015. Distinct roles for GABA across multiple timescales in mammalian circadian timekeeping. *Proceedings of the National Academy of Sciences*, 112(29), pp.E3911–E3919.

Froy, O. et al., 2003. Illuminating the circadian clock in monarch butterfly migration. *Science*, 300(5623), pp.1303–1305.

Guerra, P.A. et al., 2012. Discordant timing between antennae disrupts sun compass orientation in migratory monarch butterflies. *Nature communications*, 3, p.958.

Guerra, P.A. & Reppert, S.M., 2013. Coldness triggers northward flight in remigrant monarch butterflies. *Current Biology*, 23(5), pp.419–423.

Heinze, S. et al., 2013. Anatomical basis of sun compass navigation II: the neuronal composition of the central complex of the monarch butterfly. *Journal of Comparative Neurology*, 521(2), pp.267–298.

Heinze, S. & Reppert, S.M., 2012. Anatomical basis of sun compass navigation I: the general layout of the monarch butterfly brain. *Journal of Comparative Neurology*, 520(8), pp.1599–1628.

Heinze, S. & Reppert, S.M., 2011. Sun compass integration of skylight cues in migratory monarch butterflies. *Neuron*, 69(2), pp.345–358.

Merlin, C., Gegear, R.J. & Reppert, S.M., 2009. Antennal circadian clocks coordinate sun compass orientation in migratory monarch butterflies. *Science*, 325(5948), pp.1700–1704.

Mouritsen, H. & Frost, B.J., 2002. Virtual migration in tethered flying monarch butterflies reveals their orientation mechanisms. *Proceedings of the National Academy of Sciences*, 99(15), pp.10162–10166.

Myung, J. et al., 2015. GABA-mediated repulsive coupling between circadian clock neurons in the SCN encodes seasonal time. *Proceedings of the National Academy of Sciences*, p.201421200.

Neri, P., 2006. Spatial Integration of Optic Flow Signals in Fly Motion-Sensitive Neurons. *Journal of Neurophysiology*, 95(3), pp.1608–1619.

Pedrotti, F.L., Pedrotti, L.S. & Pedrotti, L.M., 1993. *Introduction to optics*, Prentice-Hall Englewood Cliffs.

Tammero, L.F., Frye, M.A. & Dickinson, M.H., 2004. Spatial organization of visuomotor reflexes in Drosophila. *J Exp Biol*, 207(Pt 1), pp.113–122.

Tanoue, S. et al., 2004. Circadian clocks in antennal neurons are necessary and sufficient for olfaction rhythms in Drosophila. *Current Biology*, 14(8), pp.638–649.

Ukai-Tadenuma, M., Kasukawa, T. & Ueda, H.R., 2008. Proof-by-synthesis of the transcriptional logic of mammalian circadian clocks. *Nature Cell Biology*, 10(10), pp.1154–1163.

Zhu, H. et al., 2008. Cryptochromes define a novel circadian clock mechanism in monarch butterflies that may underlie sun compass navigation. *PLoS biology*, 6(1).

Zhu, H. et al., 2009. Defining behavioral and molecular differences between summer and migratory monarch butterflies. *BMC biology*, 7(1), p.14.

Figures Captions
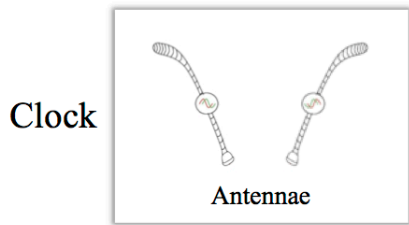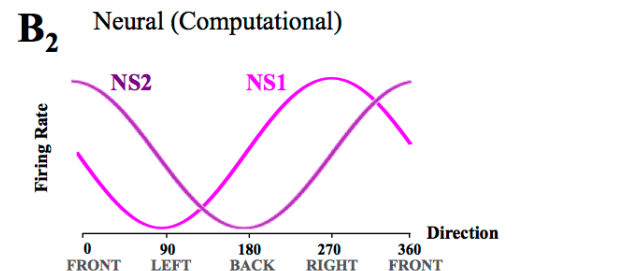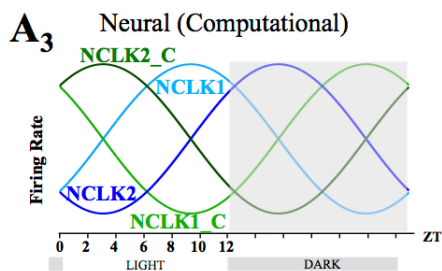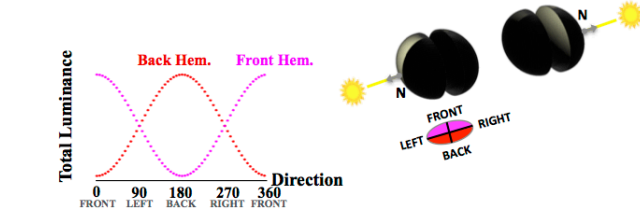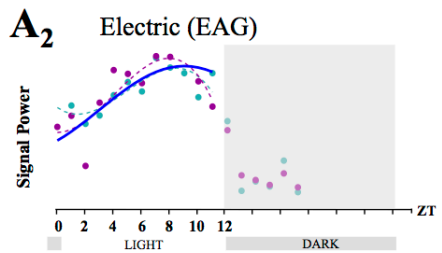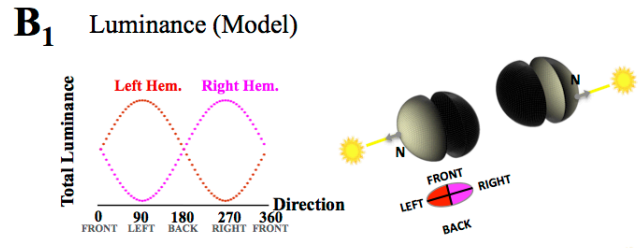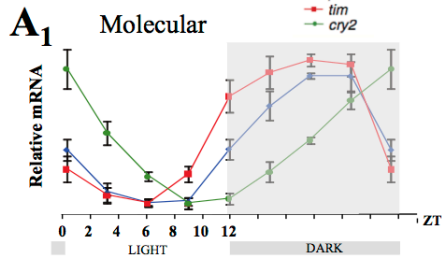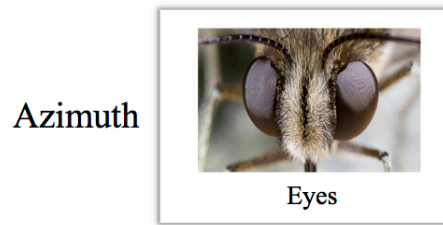
Fig. 1. Circadian and solar azimuth signals. A₁: Molecular time course curves involved in keeping the circadian rhythm. The per/tim/cry2 (blue/red/ green) relative mRNA levels measured in the antennae, reproduced from Fig. 2 in (Merlin et al. 2009). **A₂:** Signals recorded from the antenna using EAG over two days (D1-cyan, D2-magenta; normal L:D(12:12) regime; freq. > 65 Hz). Points in each light segment are fitted with a 3rd order polynomial fit (dashed curves) and globally with a cosine fit (solid blue curve: $max = 9\ ZT, min = 18\ ZT$). **A₃:** Firing rate profiles of neurons NCLK1_C (light green; accords with cry2), NCLK1 (cyan) and NCLK2_C(dark green), NCLK2 (navy; accords with per/tim). **B:** "The Butterfly eyes"; *Graphium cloanthus kuge* butterfly eyes reflecting the direction of the light; Credit: S. Yung (source: Flickr). **B₁:** Luminance of rotating light source captured by two hemispheres that model the monarch eyes. **B₁** top:

Luminance captured by left/right hemispheres. **B₁** bottom: Luminance captured by back/front hemispheres. **B₂:** Firing rate curves of NS1 and NS2 neurons which receptive fields cover the right and the front hemisphere respectively.
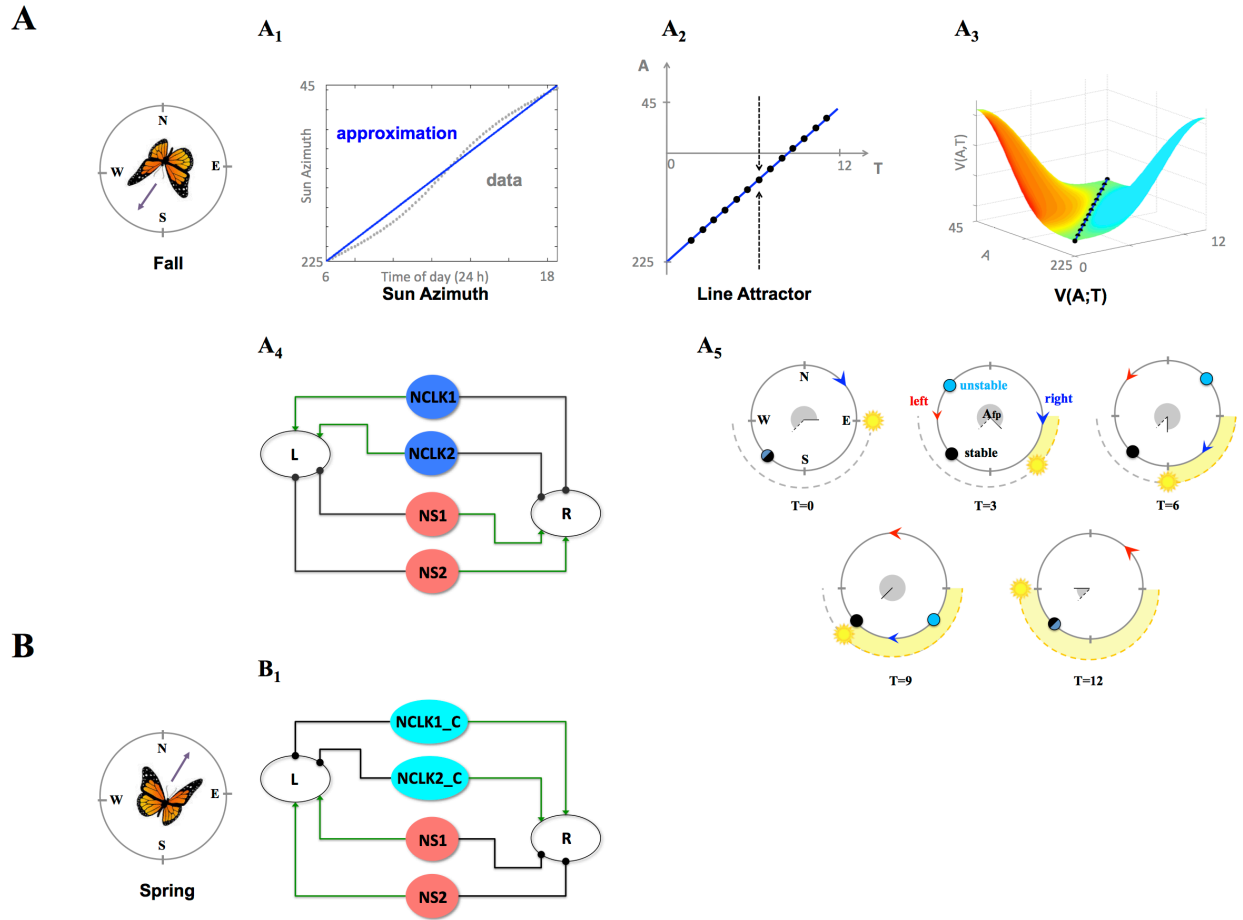
Fig. 2. Integration mechanism for flight orientation control. A: Fall migration to the SW direction. **A₁:** SW measurements (early fall, MA, USA from USNO) with respect to the solar azimuth (gray). Line approximation (A_{fp}) to these points (blue). **A₂:** Control requirements for the line-attractor: all points in the plane will converge to the SW. **A₃:** Potential (Lyapunov) function $V(A,T)$ that determines the direction of the change of the angular position for each point in (T,A) plane. As required, $V(A,T) > 0$ everywhere except on the line attractor. Its derivative, $\partial V(A,T)/\partial A$, points toward the line attractor. **A₄:** Input wiring diagram of L and R neurons indicative into which direction to turn. Such wiring produces the function $V(A;T)$ which guarantees a line attractor. **A₅:** Angular position of fixed points (stable-black, unstable-cyan), directions of correction of flight (blue-right, red-left) and the angle A_{fp} (gray) in the compass view at different times of day ($T = 0,3,6,9,12$). **B:** Reflected integration circuit (NCLK1_C, NCLK2_C replace NCLK1, NCLK2; sign of connections is flipped) produces a circuit that keeps the NE flight direction (used in spring migration).

17

A

unstable (separatrix)
stable (balanced)
V of current angle

(t = 2s)   (t = 6s)
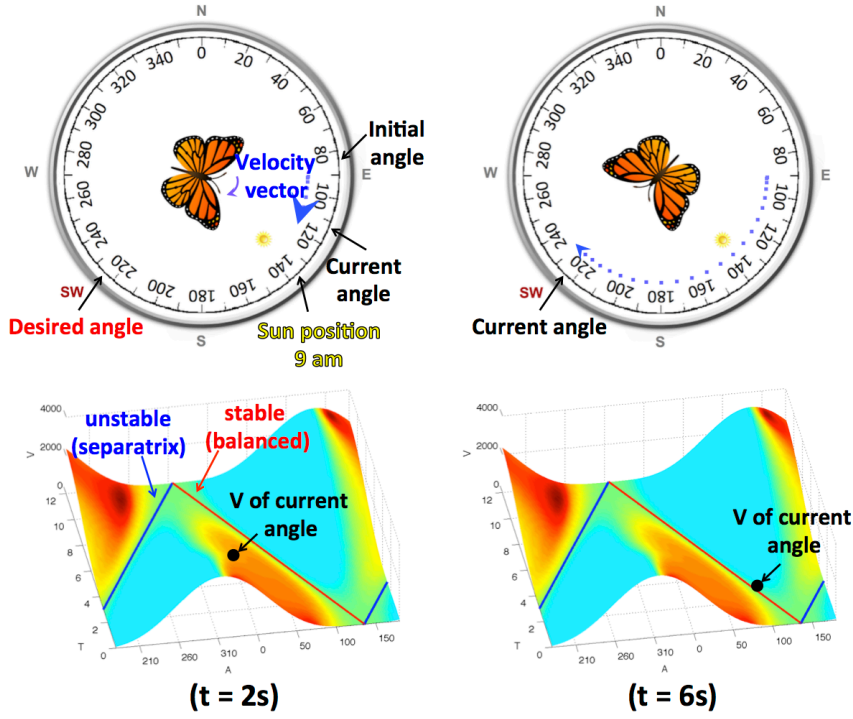
B **Morning** 9 am (ZT=3)

Afternoon 3 pm (ZT=9)

(t = 2s)   (t = 8.5s)   (t = 11.5s)   (t = 25s)
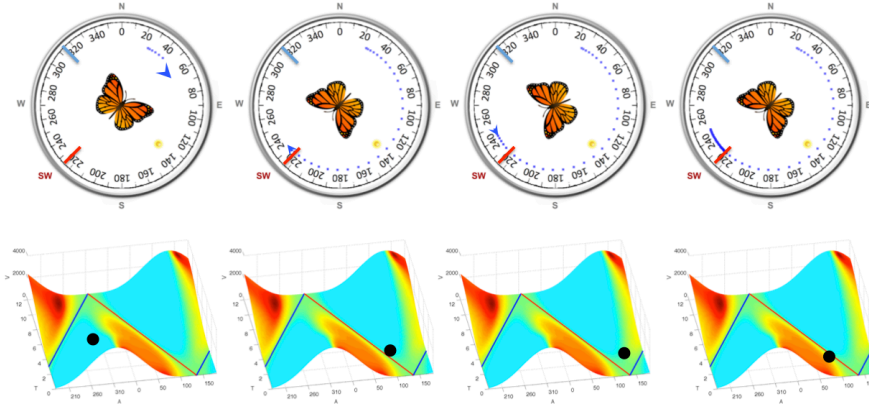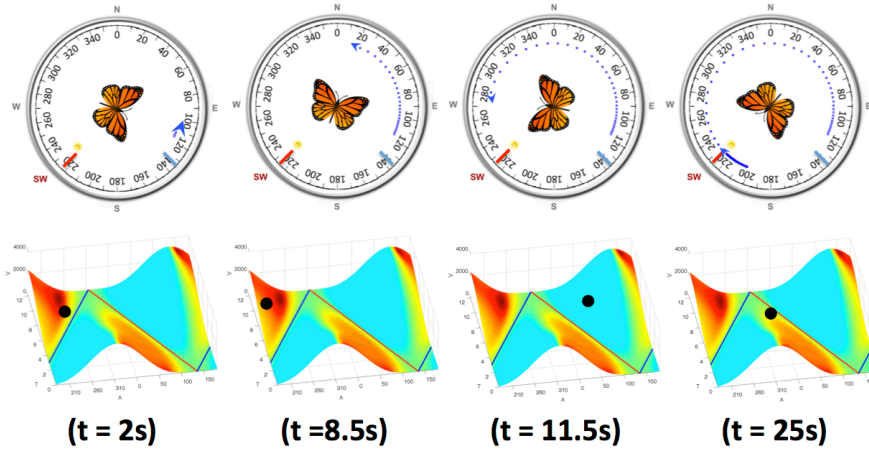
Fig. 3. Flight tracks simulator. A: Simulated flight tracks in a compass view (top), with the sun at an angular position according to time of day (here $ZT = 3:9am$). The butterfly rotates to find the SW. Rotation angle is sampled every $0.3\ sec$ and marked by blue dots. Simulated flight tracks projected on the potential function $V(A,T)$ (bottom). The black ball marks the current potential. As time progresses, the ball slides on the surface of the potential function toward the fixed point located on the stable line of fixed points (red) without crossing the separatrix line (blue). **B:** Illustration of convergence to the SW from rest and initial angular position $110°$ to the left of the sun, sampled at $t = 2, 8.5, 11.5, 25\ sec$. In the morning scenario (top), initial position falls on the right of the separatrix (cyan bar) and is followed by rightward rotation to the SW (red bar). In the afternoon scenario (bottom), initial position falls on the left of the separatrix, and followed by leftward rotation to the SW, produces a longer cycle, unlike the morning scenario.
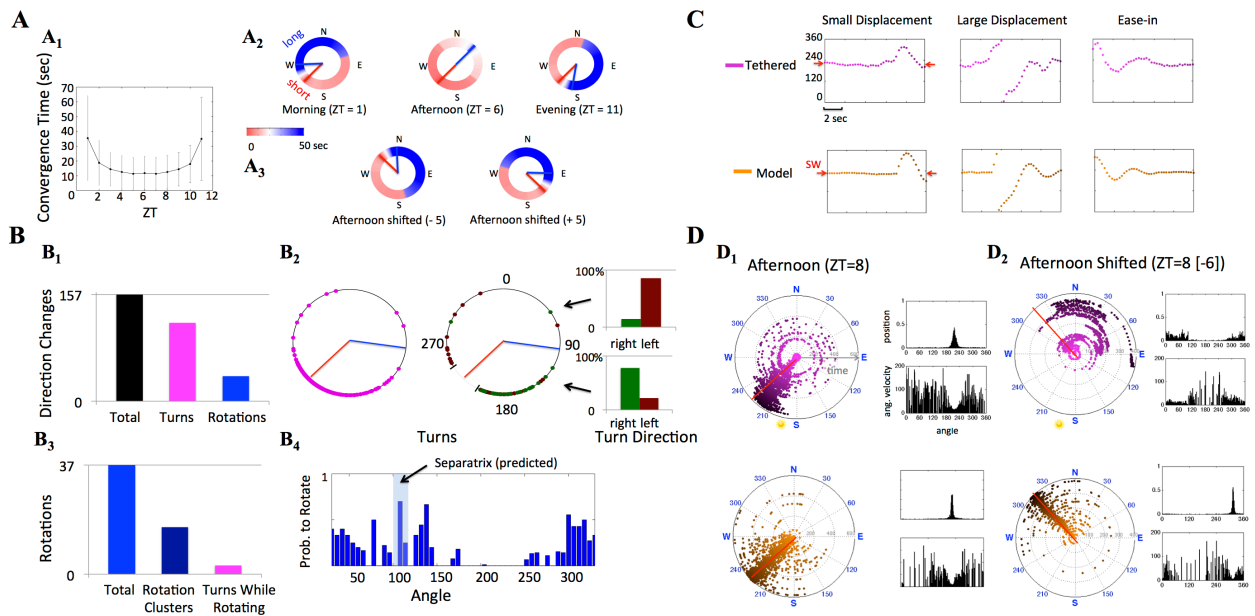
Fig. 4. Model simulated flight angle tracks compared with tethered flight.

A$_1$: Mean timescales for convergence to the SW in the model starting at rest from uniformly distributed angular positions (5° bins) computed at different times of day. **A$_2$**: Spatial distribution of convergence timescales at three times of day. **A$_3$**: Spatial distributions in the afternoon ($ZT = 6$) with shifted L:D cycle by -5h or +5h; analogous to morning/evening distributions rotated by 90° clockwise/counterclockwise. **B:** Changes of direction (turns/rotations) analyzed from raw data recorded in (Guerra et al. 2012). See Fig 4S for particular data sets used here. **B$_1$:** Direction changes in flight tracks. **B$_2$:** Spatial distribution of turns. Each turn is marked by magenta dot or according to their direction, green: left; red: right. Red and blue radii denote the positions of predicted stable and separatrix fixed points. **B$_3$**: Rotations count. **B$_4$**: Probability for full rotation (within ± 2 sec) from uniformly distributed angular positions (6° bins). **C**: Typical flight signatures ($10\ sec$ duration) within recorded (top) and model (for $ZT = 8$) (bottom) tracks; In the model, displacement is achieved by perturbing the input force until angular position reaches 300°(small), 15°(large) or 65°(ease-in). **D**: Tracks for long period of flight ($10\ min$) in a radial plot (time is the radius) and statistics of the angle / angular velocity. **D$_1$**: Flight track in the afternoon for a monarch with regular L:D cycle (L is 6am:6pm). **D$_2$**: Flight track in the afternoon for a monarch with an adjusted L:D cycle by 6h backward (L is 12pm:12am).